Efficient excitation and collection of single-molecule fluorescence close to a dielectric microsphere

Davy Gérard,[1,2,3] Alexis Devilez,[1] Heykel Aouani,[1] Brian Stout,[1] Nicolas Bonod,[1] Jérôme Wenger,[1,*] Evgeny Popov,[1] and Hervé Rigneault[1]

[1]*Institut Fresnel, CNRS, Aix-Marseille Université, Ecole Centrale Marseille, Campus de Saint-Jérôme, 13013 Marseille, France*

[2]*Present address: Laboratoire de Nanotechnologie et d'Instrumentation Optique, Institut Charles Delaunay, Université de Technologie de Troyes, France*

[3] *davy.gerard@utt.fr*

**Corresponding author: jerome.wenger@fresnel.fr*

Received April 20, 2009; accepted May 28, 2009;
posted June 4, 2009 (Doc. ID 110228); published June 30, 2009

Dielectric microspheres illuminated by a tightly focused Gaussian beam can focus light on a tiny spot with subwavelength dimensions along the three directions of space. We report here a detailed experimental and theoretical study of the interaction between a single fluorescent molecule and this peculiar electromagnetic distribution. The microsphere increases the excitation intensity sensed by the molecule up to a factor of 2.2, while at the same time it allows for a collection efficiency of up to 60% by redirecting the light emitted at large incidences toward the optical axis. By combining these two effects, the number of collected fluorescence photons can be increased up to a factor of 5. We quantify the evolution of the excitation and collection contributions with the microsphere dimensions and compare our experimental findings with numerical simulations.

OCIS codes: 260.2510, 240.3990, 170.6280, 350.3950, 290.4020.

1. INTRODUCTION

A crucial issue for many applications in biophotonics is to enhance the detected signal of fluorescent molecules or quantum dots. This can be done by increasing the local excitation intensity, the emission rate, or the radiation collection efficiency. All these properties can be controlled by properly tailoring the electromagnetic environment [1]; microstructures and nanostructures thus offer new opportunities for highly efficient detection of single emitters. In this perspective, strong attention has been devoted to metallic nanostructures (see [2,3] for reviews). These structures are known to generate strong electromagnetic fields in their vicinity, allowing a more efficient excitation of molecules. However, metals are also known to quench the fluorescence or luminescence emission, and a delicate balance has to be found between field enhancement and losses [4,5].

An alternative to enhancing the excitation intensity is to improve the detected fluorescence by increasing the collection efficiency. Already, a flat dielectric interface significantly modifies the angular emission of a dipole if the emitter is sufficiently close to the interface [6–8]. For a dipole bound to a glass–water interface with averaged dipole orientations, up to 72% of the total fluorescence is emitted into the glass half-space of refractive index 1.5. However, the angular distribution shows a significant emission maximum around the direction of the critical angle of total internal reflection, with about 34% of the fluorescence being emitted into the glass above the critical angle [9–11]. This radiation is not collected by classical microscope objectives and is therefore called forbidden light [8]. To achieve fluorescence collection efficiencies of more than 50%, it is necessary to collect light above the critical angle, as done for instance by a parabolic collector [9,10,12] or by a solid immersion lens [13–15].

In a recent publication [16], we have shown that dielectric microspheres can be a viable alternative for enhanced fluorescence detection in solution. When a latex microsphere is illuminated with a tightly focused Gaussian beam, it overfocuses light in a region with subwavelength dimensions in both the transverse and longitudinal directions, creating high local intensities (see Fig. 1, right panel). This effect stems from interferences between the field scattered by the sphere and the high angular components of the incident Gaussian beam passing aside the sphere [17]. Microspheres therefore appear as an attractive and cost-effective route to enhance the fluorescence emission up to five times without requiring expensive nanofabrication facilities. Let us point out that this phenomenon differs from the so-called "photonic nanojets" arising when a dielectric microsphere is illuminated by a plane wave [18–20]. Under plane wave illumination, no subwavelength confinement is obtained along the axial direction, and thus the resulting focal volume does not outperform the diffraction limit obtained with a high numerical aperture (NA) objective. This largely lowers the interest of such standard nanojets for fluorescence detection.

In this Letter, we provide a detailed experimental and theoretical analysis of the interaction between an emitter

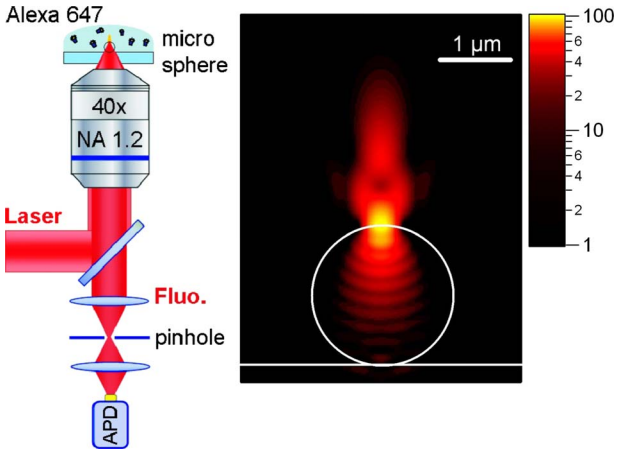

Fig. 1. (Color online) Schematic view of the experimental setup for confocal single molecule detection enhanced by a single microsphere (left panel) and numerical simulation of the electric field intensity distribution near a dielectric microsphere (diameter 2 μm, refractive index 1.59) illuminated with a tightly focused Gaussian beam at $\lambda=633$ nm with 1.2 NA (right panel, note the logarithmic scale). The outer medium refractive index is set to 1.33; the glass slide refractive index is 1.5.

and a microsphere under tightly focused Gaussian illumination. We thoroughly investigate the origins of the fluorescence enhancement close to a dielectric microsphere and quantify the gains in excitation and collection efficiencies. Both experimental observations and numerical simulations show that the microsphere increases the excitation intensity sensed by the molecule up to a factor of 2.2, while at the same time it allows for a gain in collection efficiency up to 60% by redirecting the light emitted at large incidences toward the optical axis.

2. EXCITATION AND COLLECTION EFFICIENCIES CHARACTERIZATION

The presence of a microsphere affects the fluorescence signal via three phenomena: (i) local enhancement of the excitation intensity inside the focused spot, (ii) improvement of the emitter's quantum yield, and (iii) modification of the emitter's radiation pattern, directing more energy toward the detectors. We have recently developed an experimental procedure to distinguish between the respective weights of these contributions by employing fluorescence correlation spectroscopy (FCS) combined with fluorescence lifetime measurements. This procedure has already been used to quantify the fluorescence alteration by gold nanometric apertures [21] and is briefly reviewed here.

In steady state, the detected fluorescence count rate per molecule (CRM) is given by [22]

$$\mathrm{CRM} = \kappa\phi\frac{\sigma I_e}{1+I_e/I_s}, \tag{1}$$

where κ is the fluorescence collection efficiency and $\phi = k_{\mathrm{rad}}/k_{\mathrm{tot}}$ is the quantum yield with k_{rad} as the radiative emission decay rate and k_{tot} as the total decay rate. σ is the absorption cross section, I_e is the excitation intensity, and $I_s \propto (k_{\mathrm{tot}}/\sigma)$ is the saturation intensity. Please note that the I_e and I_s are given here as the number of photons per second and per surface unit. The FCS technique allows one to reliably estimate this CRM, which corresponds to the average number of photons emitted by a single molecule [22,23].

The fluorescence enhancement η_F near a microsphere is defined as the ratio of the detected fluorescence CRM near the microsphere with respect to the open solution for a fixed excitation power, $\eta_F = \mathrm{CRM}_{\mathrm{sphere}}/\mathrm{CRM}_{\mathrm{sol}}$. Let us consider the two extreme excitation regimes depending on the relative values of I_e and I_s. In the low excitation regime $I_e \ll I_s$, the CRM and the fluorescence enhancement reduces to

$$\mathrm{CRM}_{\mathrm{low}} = \kappa\phi\sigma I_e \quad (I_e \ll I_s), \tag{2}$$

$$\eta_{F,\mathrm{low}} = \eta_\kappa \eta_\phi \eta_{I_e} \quad (I_e \ll I_s), \tag{3}$$

where η_κ, η_ϕ, and η_{I_e} are the enhancements in the collection efficiency, quantum yield, and excitation rate, respectively. In the saturation regime $I_e \gg I_s$, the dependence on the excitation intensity disappears in Eq. (1), and the fluorescence rate enhancement is expressed [21] as

$$\eta_{F,\mathrm{sat}} = \eta_\kappa \eta_{k_{\mathrm{rad}}} \quad (I_e \gg I_s), \tag{4}$$

which indicates that the fluorescence enhancement at saturation is determined only by the gains in collection efficiency η_κ and radiative emission rate $\eta_{k_{\mathrm{rad}}}$.

In our specific case, it is possible to further simplify the above equations. A nonabsorbing dielectric microstructure is expected to only marginally modify the dye's photophysics, since the absence of absorption losses does not open new nonradiative deexcitation routes. We confirm this assumption by the report in Section 4 of experimental evidence based on time-correlated fluorescence measurements that the fluorescence lifetime of the dye is not affected by the presence of the microsphere. Consequently, we consider that $\eta_{k_{\mathrm{rad}}} = \eta_\phi = 1$. Equations (3) and (4) then become

$$\eta_{F,\mathrm{low}} = \eta_\kappa \eta_{I_e} \quad (I_e \ll I_s), \tag{5}$$

$$\eta_{F,\mathrm{sat}} = \eta_\kappa \quad (I_e \gg I_s). \tag{6}$$

This set of equations provides the guidelines for distinguishing between the gains in collection efficiency η_κ and excitation intensity η_{I_e} brought by the photonic structure. The procedure can be summarized as follows: the fluorescence rates per molecule CRM are measured by FCS for increasing excitation powers in open solution and in the case of a microsphere. The resulting data points are fitted according to Eq. (1) to deduce the fluorescence enhancements $\eta_{F,\mathrm{low}}$ and $\eta_{F,\mathrm{sat}}$ taken at the asymptotic limits where $I_e \to 0$ and $I_e \to \infty$, respectively. According to Eq. (6), the value of $\eta_{F,\mathrm{sat}}$ at saturation gives the collection efficiency enhancement η_κ. The excitation intensity enhancement is obtained as $\eta_{I_e} = \eta_{F,\mathrm{low}}/\eta_{F,\mathrm{sat}}$ [Eq. (5)]. This unambiguously separates the excitation and emission contributions to the total fluorescence enhancement.

3. EXPERIMENTAL METHODS

Our experimental setup is based on an inverted confocal microscope with a NA=1.2 water-immersion objective (Fig. 1, left panel). A single latex microsphere of well calibrated diameter (Fluka Chemie GmBH: d_s=1, 1.5, 2, or 3 μm; dispersion <0.1%; refractive index 1.59) is set at the microscope objective focus with nanometer resolution using a three axis piezoelectric stage. For the microsphere sample preparation, the spheres are diluted in pure water and dispersed on a cleaned microscope glass coverslip before air drying to ensure adhesion to the substrate. The concentration is set to isolate a single sphere per 10 μm $\times$10 μm. Adhesion onto the glass surface is sufficient to ensure that the sphere remained stuck on the substrate for the duration of the experiment.

A 50 μL droplet of Alexa Fluor 647 fluorescent molecules diluted in pure water to a concentration of 40 nM is deposited on top of the microsphere sample. Alexa Fluor 647 are purchased from Invitrogen, Carlsbad, Calif., and have peak absorption and emission at 650 and 668 nm, respectively. The molecules are excited by a linearly polarized He–Ne laser beam at 633 nm focused by the combination of the microscope objective and the microsphere. The backward-emitted fluorescence is collected via the same combination of microsphere and microscope objective, and filtered from the scattered laser light by a dichroic mirror (Omega Filters 650DRLP) and a long-pass filter (Omega Filters 640AELP). A 30 μm confocal pinhole conjugated to the microscope objective focal plane rejects out-of-focus light. After the pinhole, the fluorescence is detected by an avalanche photodiode with 670±20 nm bandpass filter (Omega Filters 670DF40).

For FCS, the fluorescence intensity temporal fluctuations $F(t)$ are analyzed by a hardware correlator (ALV-GmbH ALV6000) to compute the temporal correlation, $g^{(2)}(\tau)=\langle F(t)F(t+\tau)\rangle/\langle F(t)\rangle^2$, where $\langle\ \rangle$ stands for time averaging over the experiment duration [22,23]. Each FCS measurement is obtained by averaging ten runs of 10 s duration. Numerical fit of the FCS data provides the average number of molecules N and, therefore, the fluorescence CRM. We refer the reader to [16] for a detailed discussion on FCS analysis close to a latex microsphere.

For lifetime measurements, we use a time-correlated single photon counting card (PicoQuant PicoHarp 300). The excitation is switched to a picosecond laser diode operating at 636 nm. Perfect spatial overlap between the modes of the pulsed laser diode and the CW He–Ne laser is obtained by coupling to a single-mode optical fiber prior to focusing in the microscope [21]. Overall, the temporal resolution of the setup is 120 ps, well below the 1.0 ns fluorescence lifetime recorded for Alexa Fluor 647 in water solution.

We emphasize that the value of the fluorescence enhancement is extremely sensitive to the position of the microsphere. An accurate positioning of the focus with ±150 nm precision is required along the axial direction [16]. In what follows we only present the results obtained at the optimal position. Note that the values for each diameter have been averaged over several microspheres to ensure the reproducibility of the results. Finally, let us point out that owing to the statistical approach used here, all our results have to be understood as spatially averaged values over all the possible molecular orientations and positions inside the confocal detection volume.

4. RESULTS AND DISCUSSION

Figure 2(a) shows the measured CRMs versus the excitation power for the different sphere diameters and for the reference case in free solution. Solid curves indicate numerical fits using Eq. (1), which stand in good agreement with the experimental data. CRM enhancements with the different microsphere diameters are clearly observed at all excitation powers. Let us also emphasize that CRMs larger than 100 kHz are readily obtained with the microsphere, while these values remain unreachable in free solution. From the numerical fits we deduce the values of the fluorescence enhancement factors in the limits of low excitation $\eta_{F,\mathrm{low}}$ and saturation $\eta_{F,\mathrm{sat}}$. The results are displayed in Fig. 2(b) versus the sphere diameter, showing an optimum for a diameter of 1.5 μm. It is worth noticing that with a 1.5 μm latex microsphere it is possible to reach a five times enhancement of the molecular fluorescence, a value that is comparable to the enhancement factors reported with some metallic nanostructures [3].

Along with FCS experiments, we perform fluorescence lifetime measurements to quantify the alteration of the molecule total decay rate close to the microsphere. Typical decay curves are plotted in Fig. 3 in the case of the reference solution [black dots (free solution)] and for a 2 μm diameter sphere (red dots). A numerical fit taking into account the 120 ps instrument resolution indicates a lifetime reduction near the sphere of less than 4%. For the other sphere diameters, we observed even smaller varia-

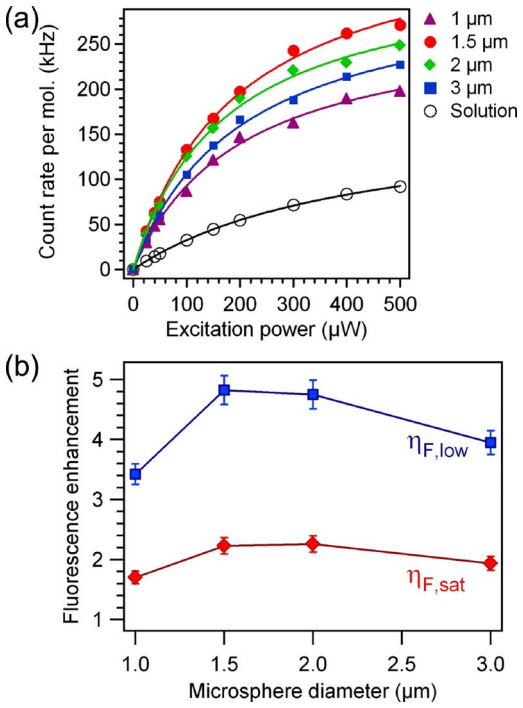

Fig. 2. (Color online) (a) CRM versus excitation power for the different sphere diameters and for the reference solution. Dots: experimental data; solid curves: numerical fit using Eq. (1). (b) Fluorescence enhancement factors in the low excitation regime $\eta_{F,\mathrm{low}}$ and at saturation $\eta_{F,\mathrm{sat}}$, as deduced from the numerical fits in (a).

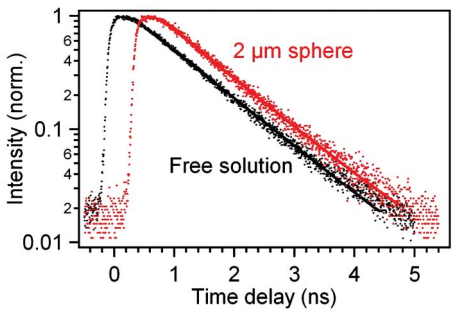

Fig. 3. (Color online) Fluorescence lifetime measurements. Dots: experimental data; solid curves: numerical fits taking into account the resolution of the setup. The curves are horizontally shifted for clarity.

tions in the fluorescence lifetime, which are limited by the statistical accuracy of our measurements. Thus, we consider that for the range of diameters tested here, the microsphere has a negligible influence on the fluorescence lifetime. Since the nonabsorbing microsphere obviously does not open new nonradiative de-excitation routes, our observations of an unchanged fluorescence lifetime mean that the dye's radiative rate and consequently its quantum yield are also unaffected by the microsphere. This validates the assumption $\eta_{k_{\mathrm{rad}}}=\eta_{\phi}=1$ made in Section 2.

We can now distinguish the excitation and emission contributions to the overall fluorescence enhancement. Following Eq. (6), the collection efficiency enhancement η_{κ} is given by the value of $\eta_{F,\mathrm{sat}}$ at saturation. The excitation intensity enhancement is obtained as $\eta_{I_e}=\eta_{F,\mathrm{low}}/\eta_{F,\mathrm{sat}}$ [Eq. (5)]. According to this procedure, Fig. 4 shows the excitation and collection enhancement factors corresponding to the experimental results in Fig. 2(b). It appears from these results that excitation and collection effects are both involved in the global fluorescence enhancement. For the optimal microsphere diameter of 1.5 μm, the excitation intensity sensed by the molecule is enhanced by a factor of 2.2, while at the same time the collection efficiency is increased by the same factor. Given the collection efficiency of 30% for the 1.2 NA objective with no microsphere, the enhancement brought by the microsphere amounts to a collection efficiency of about 66%. Such a large collection efficiency can only be obtained by redirecting the so-called forbidden light emitted at large incidence angles toward the optical axis [8,10], which shows that the microsphere acts as an efficient light collector. The microsphere can thus be seen as a microlens placed in the emitter's near field, allowing a more efficient focusing of the incident beam as well as increasing the collection of the fluorescence light.

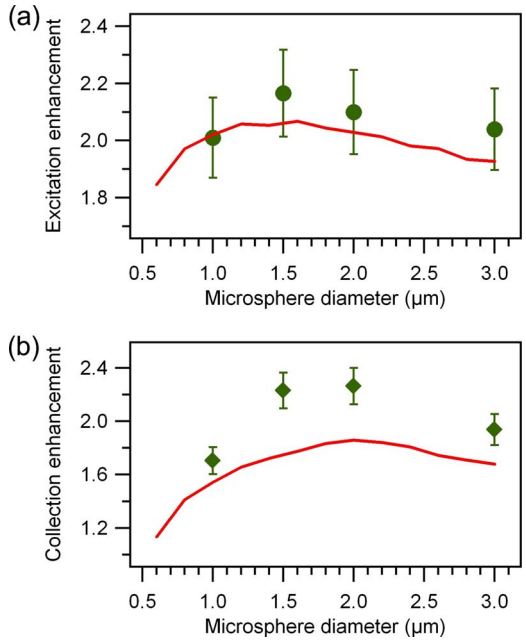

Fig. 4. (Color online) Contributions of (a) excitation and (b) collection enhancements close to a single microsphere (random dipole orientation). Markers are experimental data; curves result from numerical computation (see text).

To support the experimental data, we perform three-dimensional numerical simulations of the field distribution near a microsphere using the Lorentz–Mie theory [24]. The incident linearly polarized Gaussian beam is simulated using first-order Davis coefficients with the beam shape parameter corresponding to the experimental configuration of NA=1.2 [17]. A typical electromagnetic field intensity distribution in the case of a 2 μm diameter sphere is plotted on the right panel of Fig. 1. To compute the excitation intensity enhancement, we introduce the intensity density ϱ_e as the total excitation intensity I_V per unit of effective volume V_{eff}, $\varrho_e=I_V/V_{\mathrm{eff}}$, where the excitation intensity is given by [22,25]

$$I_V=\int_V |E|^2 \mathrm{d}V, \tag{7}$$

and the effective volume is defined as

$$V_{\mathrm{eff}}=\frac{\left(\int_V |E|^2 \mathrm{d}V\right)^2}{\int_V |E|^4 \mathrm{d}V}. \tag{8}$$

The numerical integration of the field intensity is made over the region outside the microsphere where the intensity is larger than $I_{\max}/10$, with $I_{\max}$ being the maximum intensity of the excitation field. Finally, we obtain the excitation intensity enhancement as the ratio of ϱ_e for the microsphere to the reference value of ϱ_e without the sphere. The theoretical results are plotted versus the microsphere diameter in Fig. 4(a) and are found to be in good agreement with the experimental data, with a relative difference comparable to the experimental statistical errors.

To numerically compute the gain in collection efficiency brought by the microsphere, we set a single dipole close to the surface of the sphere at the position corresponding to the maximum intensity found in the excitation field distribution in Fig. 1. We compute the average Poynting vector flux in the far field over a spherical surface of 20 μm radius located underneath the microsphere, with a center at the dipole location and a maximum half-angle of 60° corresponding to the microscope objective NA. The collection efficiency is then obtained as the ratio of this Poynting vector flux to the flux computed over all directions of

space (4π sr). Finally, the collection efficiency enhancement is derived by normalizing the collection efficiency found with a microsphere to the reference one found without the sphere. To reproduce the random dipole orientation in the experimental observations, we average the collection efficiencies found for dipole orientations along each direction x, y, and z. Figure 4(b) displays our results versus the microsphere diameter. These numerical results stand again in good qualitative agreement with the experimental findings, although we did not consider spatial averaging over various dipole locations as in the FCS experiments. Altogether, the numerical simulations confirm that gains in both local excitation intensity and collection efficiency contribute in about equal parts to the overall fluorescence enhancement. These simulations also confirm the drop in the fluorescence enhancement found experimentally for microsphere diameters below 1 μm.

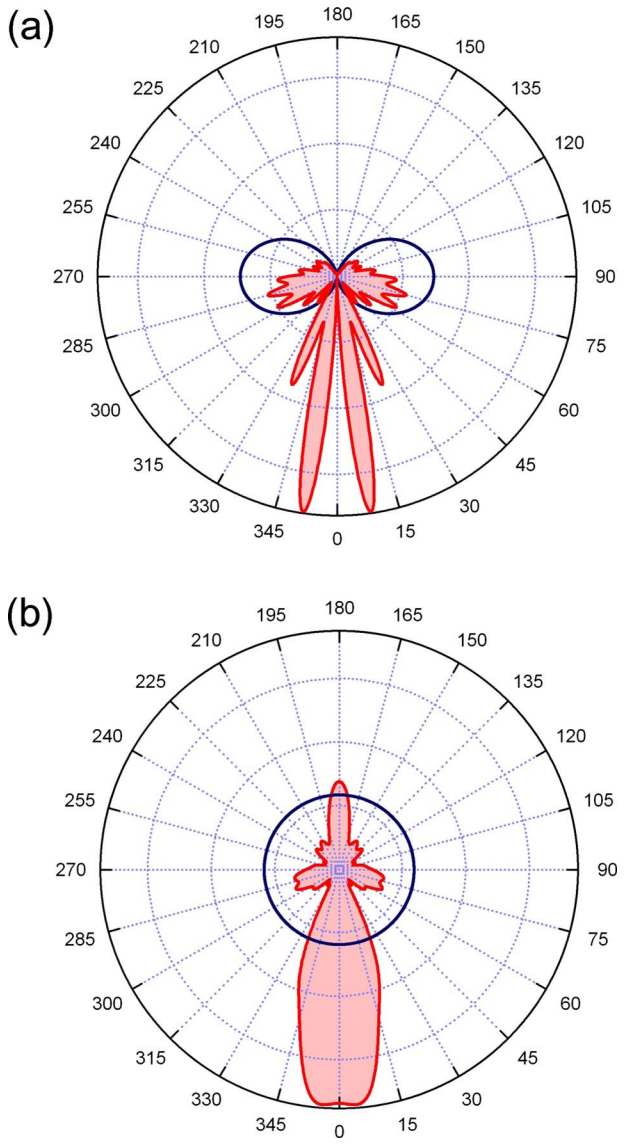

Fig. 5. (Color online) Angular distribution of the fluorescence intensity of a molecule located at 100 nm above a 2 μm polystyrene microsphere in water (red curve) for a dipole oriented along the Z axis (a) and averaged over all orientations (b). The nonfilled curves correspond to the dipole emission without the microsphere.

To illustrate the increased collection efficiency brought by the microsphere, we compute the radiation pattern for a dipole located at 100 nm on top of a 2 μm polystyrene microsphere in water. This radiation pattern is computed in the far field at a distance of 20 μm from the dipole; it fully takes into account the microsphere refractive effects. Figure 5 displays the angular distributions for a dipole oriented along the Z axis and for an average over all orientations. It is apparent that light emitted above the critical angle of 57° in the case of the polystyrene–water interface is largely redirected toward the optical axis, allowing efficient detection of the fluorescence radiation. This gives the picture of the microsphere acting as a magnifying lens directly in the emitter's vicinity.

5. CONCLUSION

We report a detailed experimental and theoretical study of the fluorescence emission alteration close to a dielectric microsphere illuminated with a tightly focused Gaussian beam. The microsphere increases the excitation intensity sensed by the emitter up to a factor of 2.2, while at the same time it allows for a collection efficiency up to 60% by redirecting the light emitted at large incidences toward the optical axis. Altogether, these effects contribute to an increase in the number of collected fluorescence photons up to a factor of 5. The microsphere is shown to act as a microlens placed in the emitter's near field, allowing a more efficient focusing of the incident beam as well as increasing the radiation collection efficiency. Let us point out that the microsphere can be designed so that the gains in excitation and collection efficiencies are maximized at the microsphere's top surface by properly choosing the microsphere radius and refractive index [17,18,26]. This extends the potential of dielectric microspheres to detect luminescent probes immobilized on the sphere surface, which can eventually be chemically functionalized [27]. Dielectric microspheres are thus found to offer a cheap, conceptually simple, and highly efficient way to enhance both excitation and harvesting of light from emitters. Further applications include optical microscopy [28], Raman spectroscopy [29], photolithography [30,31], or optical data storage [32].

ACKNOWLEDGMENT

The authors acknowledge funding from the French Centre National de la Recherche Scientifique (CNRS).

REFERENCES

1. W. L. Barnes, "Fluorescence near interfaces: the role of photonic mode density," J. Mod. Opt. **45**, 661–699 (1998).
2. J. R. Lakowicz, "Radiative decay engineering 5: metal-enhanced fluorescence and plasmon emission," Anal. Biochem. **337**, 171–194 (2005).
3. E. Fort and S. Grésillon, "Surface enhanced fluorescence," J. Phys. D **41**, 013001 (2008).
4. P. Anger, P. Bharadwaj, and L. Novotny, "Enhancement and quenching of single-molecule fluorescence," Phys. Rev. Lett. **96**, 113002 (2006).

5. R. Carminati, J.-J. Greffet, C. Henkel, and J.-M. Vigoureux, "Radiative and non-radiative decay of a single-molecule close to a metallic nanoparticle," Opt. Commun. **261**, 368–375 (2006).
6. W. Lukosz and R. E. Kunz, "Light emission by magnetic and electric dipoles close to a plane interface. I. Total radiated power," J. Opt. Soc. Am. **67**, 1607–1615 (1977).
7. W. Lukosz and R. E. Kunz, "Light emission by magnetic and electric dipoles close to a plane interface. II. Radiation patterns of perpendicular oriented dipoles," J. Opt. Soc. Am. **67**, 1615–1619 (1977).
8. L. Novotny, "Allowed and forbidden light in near-field optics. I. A single dipolar light source," J. Opt. Soc. Am. A Opt. Image Sci. Vis. **14**, 91–104 (1997).
9. J. Enderlein, T. Ruckstuhl, and S. Seeger, "Highly efficient optical detection of surface-generated fluorescence," Appl. Opt. **38**, 724–732 (1999).
10. T. Ruckstuhl, J. Enderlein, S. Jung, and S. Seeger, "Forbidden light detection from single molecules," Anal. Chem. **72**, 2117–2123 (2000).
11. J. Mertz, "Radiative absorption, fluorescence, and scattering of a classical dipole near a lossless interface: a unified description," J. Opt. Soc. Am. B **17**, 1906–1913 (2000).
12. J. Ries, T. Ruckstuhl, D. Verdes, and P. Schwille, "Supercritical angle fluorescence correlation spectroscopy," Biophys. J. **94**, 221–229 (2008).
13. K. Koyama, M. Yoshita, M. Baba, T. Suemoto, and H. Akiyama, "High collection efficiency in fluorescence microscopy with a solid immersion lens," Appl. Phys. Lett. **75**, 1667–1669 (1999).
14. A. Serov, R. Rao, M. Gösch, T. Anhut, D. Martin, R. Brunner, R. Rigler, and T. Lasser, "High light field confinement for fluorescent correlation spectroscopy using a solid immersion lens," Biosens. Bioelectron. **20**, 431–435 (2004).
15. R. Rao, J. Mitic, A. Serov, R. A. Leitgeb, and T. Lasser, "Field confinement with aberration correction for solid immersion lens based fluorescence correlation spectroscopy," Opt. Commun. **271**, 462–469 (2007).
16. D. Gérard, J. Wenger, A. Devilez, D. Gachet, B. Stout, N. Bonod, E. Popov, and H. Rigneault, "Strong electromagnetic confinement near dielectric microspheres to enhance single-molecule fluorescence," Opt. Express **16**, 15297–15303 (2008).
17. A. Devilez, N. Bonod, B. Stout, D. Gérard, J. Wenger, H. Rigneault, and E. Popov, "Three-dimensional subwavelength confinement of photonic nanojets," Opt. Express **17**, 2089–2094 (2009).
18. Z. Chen, A. Taflove, and V. Backman, "Photonic nanojet enhancement of backscattering of light by nanoparticles: a potential novel visible-light ultramicroscopy technique," Opt. Express **12**, 1214–1220 (2004).
19. A. Heifetz, K. Huang, A. V. Sahakian, X. Li, A. Taflove, and V. Backman, "Experimental confirmation of backscattering enhancement induced by a photonic jet," Appl. Phys. Lett. **89**, 221118 (2006).
20. P. Ferrand, J. Wenger, M. Pianta, H. Rigneault, A. Devilez, B. Stout, N. Bonod, and E. Popov, "Direct imaging of photonic nanojets," Opt. Express **16**, 6930–6940 (2008).
21. J. Wenger, D. Gérard, N. Bonod, E. Popov, H. Rigneault, J. Dintinger, O. Mahboub, and T. W. Ebbesen, "Emission and excitation contributions to enhanced single molecule fluorescence by gold nanometric apertures," Opt. Express **16**, 3008–3020 (2008).
22. C. Zander, J. Enderlein, and R. A. Keller, *Single-Molecule Detection in Solution—Methods and Applications* (VCH-Wiley, 2002).
23. W. W. Webb, "Fluorescence correlation spectroscopy: inception, biophysical experimentations, and prospectus," Appl. Opt. **40**, 3969–3983 (2001).
24. B. Stout, M. Nevière, and E. Popov, "Light diffraction by a three-dimensional object: differential theory," J. Opt. Soc. Am. A Opt. Image Sci. Vis. **22**, 2385–2404 (2005).
25. E. Popov, M. Nevière, J. Wenger, P.-F. Lenne, H. Rigneault, P. Chaumet, N. Bonod, J. Dintinger, and T. W. Ebbesen, "Field enhancement in single subwavelength apertures," J. Opt. Soc. Am. A Opt. Image Sci. Vis. **23**, 2342–2348 (2006).
26. A. Devilez, B. Stout, N. Bonod, and E. Popov, "Spectral analysis of three-dimensional photonic jets," Opt. Express **16**, 14200–14212 (2008).
27. J. R. Epstein and D. R. Walt, "Fluorescence-based fibre optic arrays: a universal platform for sensing," Chem. Soc. Rev. **32**, 203–214 (2003).
28. J. Wenger, D. Gérard, H. Aouani, and H. Rigneault, "Disposable microscope objective lenses for fluorescence correlation spectroscopy using latex microspheres," Anal. Chem. **80**, 6800–6804 (2008).
29. A. Desmedt, D. Talaga, and J.-L. Bruneel, "Enhancement of the Raman scattering signal due to a nanolens effect," Appl. Spectrosc. **61**, 621–623 (2007).
30. E. McLeod and C. B. Arnold, "Subwavelength direct-write nanopatterning using optically trapped microspheres," Nat. Nanotechnol. **3**, 413–417 (2008).
31. S. Li, C. Du, X. Dong, L. Shi, X. Luo, X. Wei, and Y. Zhang, "Superlens nano-patterning technology based on the distributed polystyrene spheres," Opt. Express **16**, 14397–14403 (2008).
32. S.-C. Kong, A. Sahakian, A. Taflove, and V. Backman, "Photonic nanojet-enabled optical data storage," Opt. Express **16**, 13713–13719 (2008).